Dynamical core of the Russian global NWP model: current state and further development

Vladimir Shashkin (1,2), Gordey Goyman (1), Mikhail Tolstykh (1,2)

(1) Marchuk Inst. of Numerical Mathematics/RAS, (2) Hydrometcentre of Russia.
email: vvshashkin@gmail.com, gordeygoyman@gmail.com, mtolstykh@mail.ru

1. Dynamical core of the SLAV operational model - recent developments

1.1 Brief description

- hydrostatic semi-Lagrangian semi-implicit core of own development,
- vorticity-divergence formulation, unstaggered grid,
- details in (Tolstykh et al, GMD 2017),
- variable resolution in latitude,
- current operational version with ~22 km horizontal resolution and 51 levels,
- new version with ~10 km horizontal resolution and 104 levels.

1.2 Improving parallel efficiency for new SLAV version (3600x1946x104 grid)

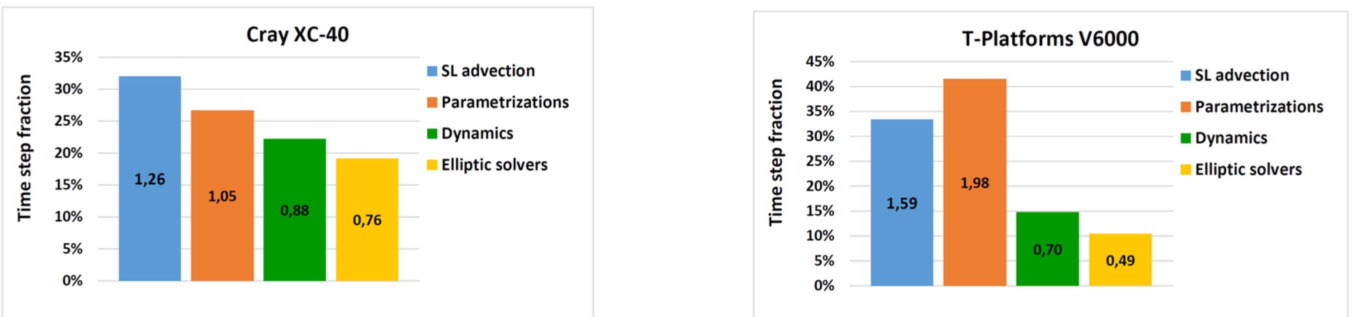

Percentage of time used in different parts of SL-AV model code while using 3888 cores of Cray XC40 (left) and 3880 cores of T-Platforms V6000 (right) systems before optimizations. Number inside the column denotes the wall-clock time of respective code part (in seconds).

Following changes are implemented:
- Single precision in semi-Lagrangian advection (except trajectories calculation)
- Single precision in transpositions
- Optimization of vector length in parameterizations

Result: 23 % elapsed time reduction

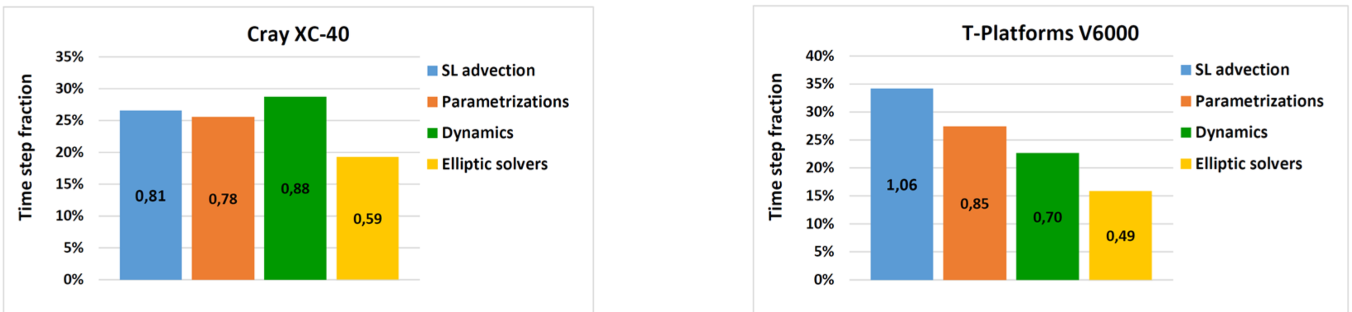

Percentage of time used in different parts of SL-AV model code while using 3888 cores at Cray XC40 (left) and 3880 cores at T-Platforms V6000 (right) after optimizations.

2. Development of dynamical core for new-generation global NWP model

2.1 Features

- compressible non-hydrostatic equation set in height-based terrain-following coordinates
- gnomonic cubed-sphere grid with nested regions of higher resolution
- reduced lat-lon grid is also a possible option
- Possible integration strategies: semi-implicit semi-Lagrangian, exponential (-SL), Runge-Kutta IMEX with Eulerian advection (all under testing in shallow-water and vertical slice Euler-eqs models)

2.2 Exponential time-integration schemes

Based on: $\dfrac{\partial \psi}{\partial t} = L\psi \;\Rightarrow\; \psi^{n+1} = \exp(L\Delta t)\psi^n$

Coupling with semi-Lagrangian (SL) advection – exclude advection operator from L => cheaper iterative exp-term integration

2.2.1 Second order exponential-Rosenbrock scheme for non-linear system

$$\frac{d\psi}{dt} = A(\psi) \rightarrow \frac{d\psi}{dt} = A(\psi^n) + J(\psi - \psi^n) + R(\psi)$$

$$J = \left.\frac{\partial A}{\partial \psi}\right|_{\psi=\psi^n}$$ - Jacobian of A at current state

$$R(\psi) = A(\psi) - A(\psi^n) - J(\psi - \psi^n)$$ - non-linear residual

$$\psi^{n+1} = \psi^n + \varphi_1(J\Delta t)(A(\psi^n)\Delta t) + O(\Delta t^2) \qquad \varphi_1(J\Delta t) = \frac{\exp(J\Delta t) - I}{J\Delta t}$$

Possible semi-Lagrangian exponential scheme: use exponential term as forcing in mid-point of upstream trajectory

$$\underbrace{\psi^{n+1}}_{\text{arrival point}} = \underbrace{\psi^{n}}_{\text{departure point}} + \underbrace{\varphi_1(J\Delta t)(A(\psi^n)\Delta t)}_{\text{midpoint}}$$

Computing *exp(J Δt)* at the midpoints (unstructured Lagrangian grid) is difficult =>
3 stage scheme:
1) SL transport D1->A by the first half of trajectory
2) Calculation of exp-like function at arrival point A
3) SL transport by the second half of trajectory D2->A

2.2.2 Phase velocities of processes with different time-integration strategies

Scheme	Advection	Fast waves
SI-SL	not retarded	retarded
SI-EUL	retarded(<=spatial discretization)	retarded
EUL-EXP	Retarded(<=spatial discretization)	not retarded
SL-EXP	not retarded	not retarded

Time integration schemes:
SI-SL – semi-implicit semi-Lagrangian   SI-EUL – semi-implicit Eulerian
EUL-EXP – exponential Eulerian   SL-EXP – semi-Lagrangian exponential

2.2.3 Shallow water experiments with different integration methods. Galewski (Tellus, 2004) case, phase I: inertia-gravity wave propagation

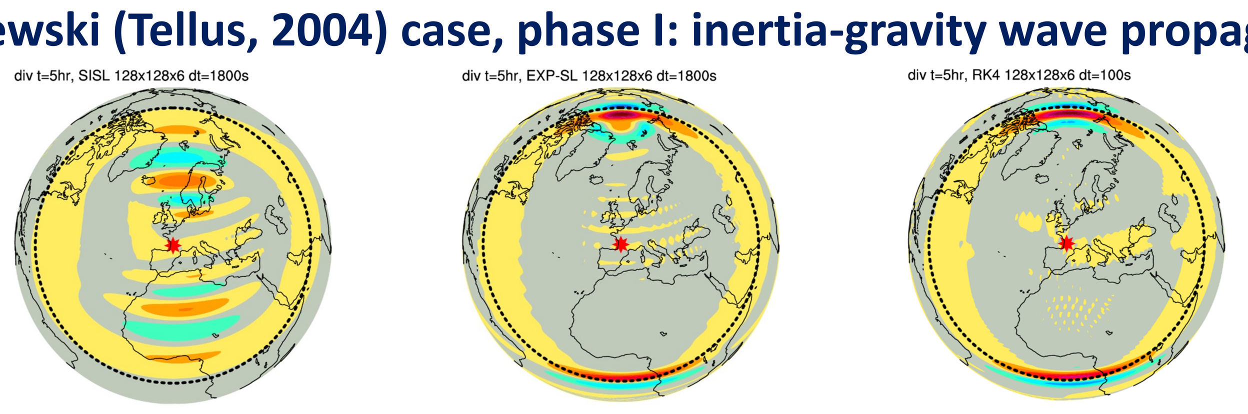

Divergence after 5hr of integration. The position of initial flow disturbance is shown by red star. Dashed circle indicates the distance of mean phase velocity multiplied by the time. SISL solution is characterized by the spurious numerical dispersion of inertia-gravity waves. EXP-SL solution is similar to the solution of explicit scheme.

2.2.4 Shallow water experiments with different integration methods. Galewski (Tellus, 2004) case, phase II: barotropic instability development

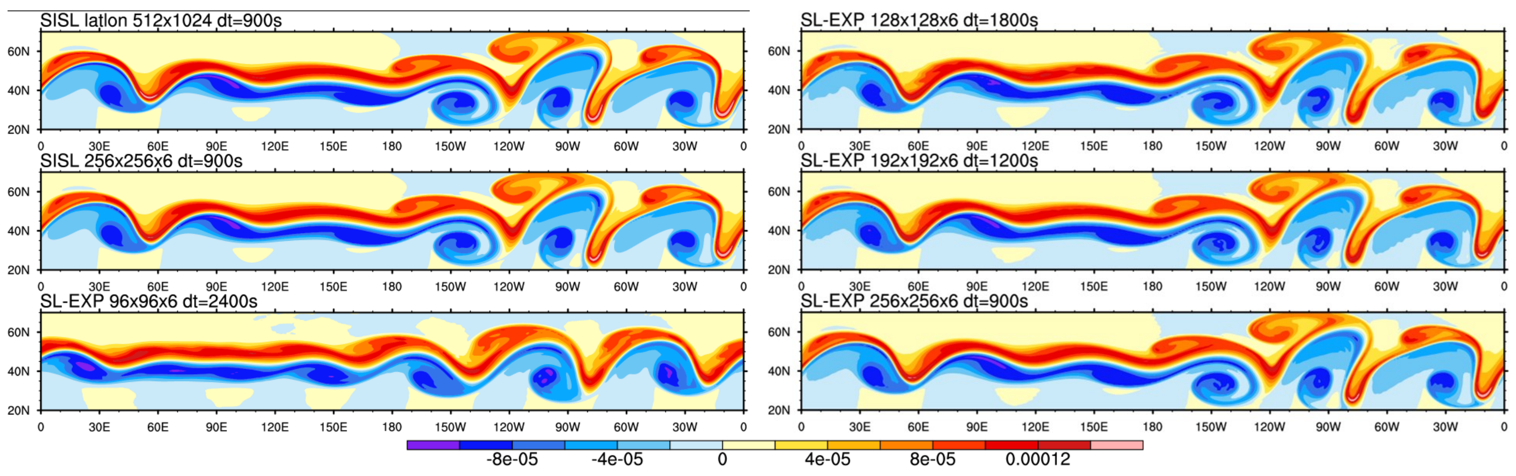

Vorticity after 6 days of integration. EXP-SL solution agrees well with the SISL solution as well as lot of published results from other SWE models.

3. Horizontal discretization at the reduced latitude-longitude grid with Arakawa C staggering

3.1 C-staggered reduced lat-lon grid design

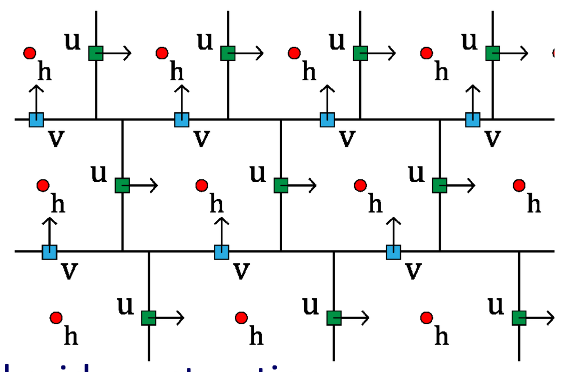

Reduced grid construction:

$$N_j^\lambda = \alpha 2N_\varphi + 2N_\varphi(1-\alpha)\frac{\cos\varphi_j - \cos\varphi_1}{\cos\frac{N_\varphi}{2} - \cos\varphi_1}$$

Here $\alpha \in (0,1]$ is the grid reduction rate.

N_φ	α	DOFs	N_1^λ	max anisotropy
16	1	1504	32	$9.8\cdot10^{-2}$
	1/2	1236	16	$2.0\cdot10^{-1}$
	1/4	1086	8	$3.9\cdot10^{-1}$
	1/8	1022	4	$7.8\cdot10^{-1}$
32	1	6080	64	$4.9\cdot10^{-2}$
	1/2	4992	32	$9.8\cdot10^{-2}$
	1/4	4420	16	$2.0\cdot10^{-1}$
	1/8	4132	8	$3.9\cdot10^{-1}$
64	1	24448	128	$2.4\cdot10^{-2}$
	1/2	20042	64	$4.9\cdot10^{-2}$
	1/4	17798	32	$9.8\cdot10^{-2}$
	1/8	16668	16	$2.0\cdot10^{-1}$
128	1	98048	256	$1.2\cdot10^{-2}$
	1/2	80304	128	$2.4\cdot10^{-2}$
	1/4	71338	64	$4.9\cdot10^{-2}$
	1/8	66858	32	$9.8\cdot10^{-2}$

Parameters of the grids used in numerical experiments

3.2 Horizontal approximation at C-staggered reduced lat-lon grid

Interpolation approach is used. Notations for the grid function values at fixed latitude

$$f_j = (f_{1,j}, \dots, f_{N_i^\lambda,i})$$

$$(\mathrm{grad}_\varphi f)_{j+\frac12} = \frac{P_{j+\frac12}^{j+1} f_{j+1} - P_{j+\frac12}^{j} f_j}{\Delta\varphi_{j+\frac12}}$$

$$(\mathrm{div}_\varphi v)_j = \frac{P_j^{j+\frac12} v_{j+\frac12}\cos\varphi_{j+\frac12} - P_j^{j-\frac12} v_{j-\frac12}\cos\varphi_{j-\frac12}}{\cos\varphi_j\Delta\varphi_j}$$

$$(fv)_j \approx \frac{1}{\cos\varphi_j}\left(S_j^{j+\frac12}(v\cos\varphi)_{j+\frac12} + S_j^{j-\frac12}(v\cos\varphi)_{j-\frac12}\right)\circ f_j$$

$$(fu)_{j+\frac12} \approx \frac{1}{\Delta\varphi_{j+\frac12}}\left(S_{j+\frac12}^{j+1}(f\circ u\Delta\varphi)_{j+1} + S_{j+\frac12}^{j}(f\circ u\Delta\varphi)_j\right)$$

Mass cons.	$\hat{1}_j^T P_j^{j+\frac12}\Delta\lambda_j = \hat{1}_{j+1}^T P_{j+1}^{j+\frac12}\Delta\lambda_{j+1}$
Energy cons. (div-grad)	$P_{j+\frac12}^{j}\Delta\lambda_{j+\frac12} = (P_j^{j+\frac12})^T\Delta\lambda_j$
Energy cons. (Coriolis)	$S_{j+\frac12}^{j}\Delta\lambda_{j+\frac12} = (S_j^{j+\frac12})^T\Delta\lambda_j$

Interpolation matrices constraints ensuring conservation properties within linear shallow-water equations spatial discretization.

Interpolation design

Prolongation:

$$P^\alpha f^\alpha = \sum_{i=1}^{n_\alpha} f_i^\alpha \psi_i^\alpha(x),\; P^\beta f^\beta = \sum_{i=1}^{n_\beta} f_i^\beta \psi_i^\beta(x)$$

Restriction:

$$(R^\alpha f)_i = \frac{\int_0^{2\pi} f(x)\varphi_i^\alpha(x)dx}{\int_0^{2\pi}\varphi_i^\alpha(x)dx},\; (R^\beta f)_i = \frac{\int_0^{2\pi} f(x)\varphi_i^\beta(x)dx}{\int_0^{2\pi}\varphi_i^\beta(x)dx}$$

Interpolation:

$$\tilde f^\beta = I_\alpha^\beta f^\alpha \equiv R_\beta P_\alpha f^\alpha,\; \tilde f^\alpha = I_\beta^\alpha f^\beta \equiv R^\alpha P^\beta f^\beta$$

Conservation properties:

$$\varphi_i^\alpha(x) = \psi_i^\alpha(x),\; \varphi_j^\beta(x) = \psi_j^\beta(x) \Rightarrow \text{energy conservation}$$

$$\sum_i \psi_i^\alpha(x) = 1,\; \sum_i \varphi_i^\beta(x) = 1 \Rightarrow \text{mass conservation.}$$

3.3 Results of numerical experiments

Three schemes:
Energy-mass conservative **`En-cons'**
Only mass conservative **`Mass-cons'**
No conservation properties **`Non-cons'**

3.3.1 Gravity waves dispersion

Spherical harmonic Y_l^m `average eigenvalue'

$$\bar\lambda_l = \frac{1}{2m+1}\sum_{m=-l}^{l}\sqrt{\frac{(LY_l^m, LY_l^m)}{(Y_l^m, Y_l^m)}},\quad l = 0\dots N_\varphi - 1$$

computed for the grids with $N_\varphi = 16$

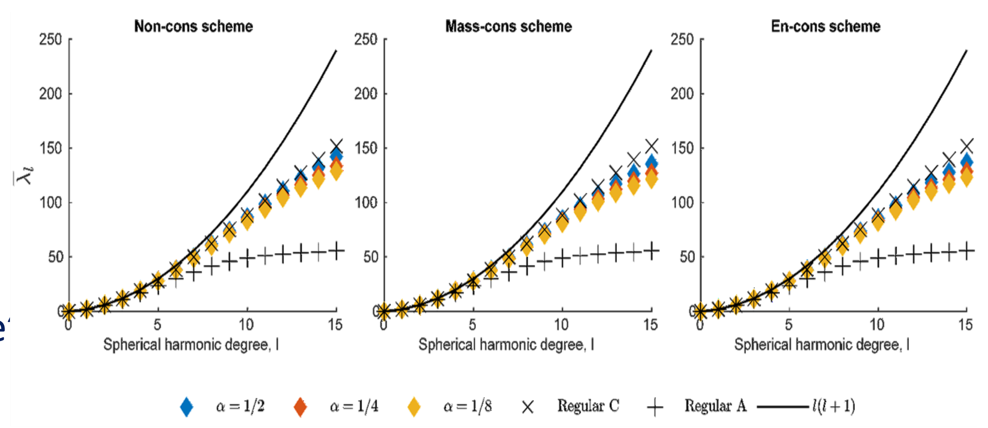

Comparison of $\bar\lambda_l$ for the different schemes.

3.3.2 Steady state solution

Linear shallow-water equations on a rotating sphere. Geostrophically balanced flow in the pole-rotated spherical coordinate system. Grids with $N_\varphi = 128$. Crank-Nicolson scheme with the iterative treatment of the Coriolis force terms. Helmholtz problem is solved using geometric multigrid preconditioned bicgstab solver.

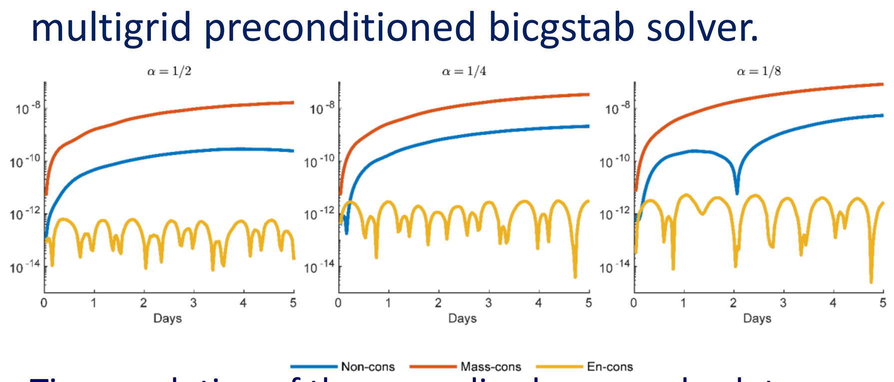

Time evolution of the normalized energy absolute error.

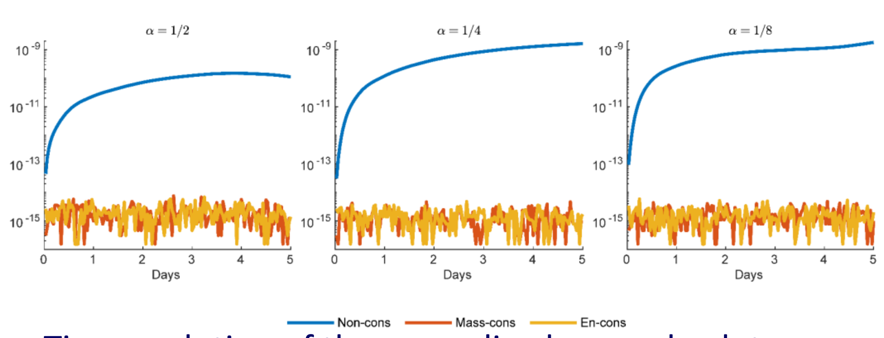

Time evolution of the normalized mass absolute error.

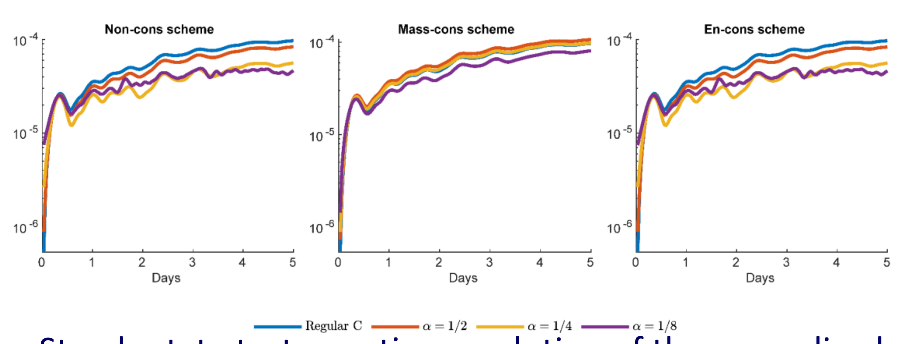

Steady state test case time evolution of the normalized l_2 height error. α is the angle of pole rotation.

4. Conclusions

1. SL advection is difficult for massively-parallel implementation, however, there are ways to reduce its cost somehow.
2. SL-exponential time-stepping and staggered reduced grid are attractive alternatives for mainstream computational methods. Further research is interesting.